

Hierarchy Composition GAN for High-fidelity Image Synthesis

Fangneng Zhan, Jiaying Huang, Shijian Lu*

Abstract—Despite the rapid progress of generative adversarial networks (GANs) in image synthesis in recent years, the existing image synthesis approaches work in either geometry domain or appearance domain alone which often introduces various synthesis artifacts. This paper presents an innovative Hierarchical Composition GAN (HIC-GAN) that incorporates image synthesis in geometry and appearance domains into an end-to-end trainable network and achieves superior synthesis realism in both domains simultaneously. We design an innovative hierarchical composition mechanism that is capable of learning realistic composition geometry and handling occlusions while multiple foreground objects are involved in image composition. In addition, we introduce a novel attention mask mechanism that guides to adapt the appearance of foreground objects which also helps to provide better training reference for learning in geometry domain. Extensive experiments on scene text image synthesis, portrait editing and indoor rendering tasks show that the proposed HIC-GAN achieves superior synthesis performance qualitatively and quantitatively.

Index Terms—Image Synthesis, Generative Adversarial Networks.

I. INTRODUCTION

AS a longstanding and fundamental challenge in computer vision research, realistic image synthesis has been attracting increasing attention since the advent of deep neural networks (DNNs). An important driving factor is the data constraint in DNNs training, where synthetic data is much cheaper, faster and more scalable as compared to the traditional manual collection approach. In recent years, the advance of generative adversarial networks (GANs) [1] opens a new door for image synthesis by iterative adversarial learning between a generator and a discriminator. Quite a number of GAN-based image synthesis systems have been reported which generate new images by direct image generation from random noises [2], image-to-image translation [3], [4] and image composition [5], [6], [7].

On the other hand, existing image synthesis systems are still facing two common constraints. First, most existing systems only strive for synthesis realism in either appearance domain or geometry domain instead of both domains. Second, many existing systems tend to sacrifice image details and resolutions and even semantics of the image contents to synthesize realistic images. Specifically, the direct generation based methods [1], [2] cannot guarantee the accurate image labels or annotations, thus the synthesized images often lack



Fig. 1. Given foreground objects of interest and a background image, the proposed HIC-GAN synthesizes realistic images in geometry and appearance domains simultaneously and is capable of handling multiple foreground objects with or without occlusions.

sufficient semantic integrity for the training of deep models. The image translation based methods [3], [4] only focuses on the synthesis realism in appearance domain with some extend of decreasing in image resolution. The composition based methods [5], [7] can generate labeled or annotated images of high-resolution, but it usually focuses on synthesis realism in geometric domain and can only deal with a single foreground object.

In our prior work [6], we proposed a spatial fusion GAN (SF-GAN) that achieves synthesis realism in both geometry and appearance domains. The SF-GAN consists of a geometry synthesizer and an appearance synthesizer. The geometry synthesizer learns the local geometry of background images with which the foreground objects can be transformed and placed into the background images unanimously. The appearance synthesizer learns to adjust the color, brightness and styles of the foreground objects to be harmonious with the background images. The two synthesizers are inter-connected as mutual references which can be trained in an end-to-end manner. On the other hand, SF-GAN is a simplified image synthesis network which assumes a single foreground object in image composition.

In this paper, we present a **H**ierarchy **C**omposition **G**AN (**HIC-GAN**) that leverages [6] but tackles a more challenging yet practical situation in image composition. Overall, HIC-GAN extends our earlier SF-GAN from three aspects. First, HIC-GAN can handle the image composition with multiple foreground objects as well as various resulting occlusions as

F. Zhan, J. Huang and S. Lu are with the School of Computer Science and Engineering, Nanyang Technological University, Singapore, 639798.

Email: {fnzhan, shijian.lu}@ntu.edu.sg, jiaying001@e.ntu.edu.sg

* indicates the corresponding author.

illustrated in Fig. 1. Second, an *attention mask mechanism* is introduced in HIC-GAN to guide the appearance adaptation of embedded foreground objects which greatly improves synthesis realism in appearance domain and also helps to provide better training reference for the learning in geometry domain. Third, we carried out several new experiments that validate the effectiveness of our new designs, and demonstrate the superior synthesis performance of HIC-GAN as compared with the state-of-the-art including our prior SF-GAN [6].

The rest of this paper is organized as follows. Section II presents related works briefly. The proposed method is then described in detail in Section III. Experimental results are further presented and discussed in Section IV. Some concluding remark is finally drawn in Section V.

II. RELATED WORK

A. Image Composition

In recent years, quite a number of image composition studies have been reported in the field of computer vision, including the synthesis of single objects [8], [9], [10], generation of full-scene images [11], [12], etc. Image composition aims to generate new images by embedding foreground objects into background images. It strives for synthesis realism by adjusting the size and orientation of the foreground objects as well as blending between foreground objects and background images. [13] proposes a model to distinguish natural photographs from automatically generated composite images. [14], [15], [16], [17], [18], [19] investigate the synthesis of scene text images for training better scene text detector and recognizer. They achieve synthesis realism by adjusting a group of parameters including text locations within the background images, geometry transformation of the foreground texts, and the fusion of the foreground texts and background images. Other image composition models have also been developed for training better DNN models [20].

The aforementioned image composition techniques strive for geometric realism by hand-crafted transformations that involve complicated parameters and are prone to unnatural geometry and alignments. The appearance realism is handled by different blending techniques where features are manually selected and susceptible to artifacts. Simple blending methods such as alpha blending [21] have been adopted to alleviate the clear appearance difference between foreground objects and background images, but they tend to blur the composed images and lose image details. Sophisticated blending such as Poisson blending [22] can achieve seamless fusion by manipulating the image gradient and adjusting the inconsistency in chrominance and luminance. Some appearance transfer based method has been reported in recent years. For example, [23] transfers the style of the foreground object according to the local statistics of the background image. [24] presents an end-to-end deep convolutional neural network for image harmonization by considering the context and semantic information of the composite images.

Our HIC-GAN adopts GAN structures to learn geometry and appearance features which produce natural and consistent image composition with minimal visual artifacts. In addition,

guided filters [25] are introduced to preserve fine image details while performing appearance fusion of foreground objects and background images.

B. Generative Adversarial Networks

GANs [1] have achieved great success in generating new images from either existing images or random noises. Instead of manually selecting features and parameters, GAN generators learn an optimal mapping from random noise or existing images to the synthesized image, while GAN discriminators differentiate the synthesized images from natural ones via adversarial learning. Quite a number of GAN-based image synthesis methods have been reported in recent years. For example, Denton et al. [26] introduces Laplacian pyramids that improve the quality of GAN-synthesized images greatly. Lee et al. [27] proposes an end-to-end trainable network for inserting an object instance mask of a specified class into the semantic label map of an image. Other systems attempt to synthesize realistic images by stacking a pair of generators [28], [29], leaning more reasonable potential features [30], exploring new training approach [2], visualizing and understanding GANs at the unit, object and scene level [31], etc.

Most existing GAN-based image systems focus on synthesis realism in appearance domain [27], [32]. For instance, CycleGAN [3] proposes a cycle-consistent adversarial network for realistic image-to-image translation, and so do other related GANs [4], [33], [34], [35], [36], [37], [38]. LR-GAN [39] synthesizes images by introducing spatial transformer networks (STNs). GP-GAN [40] synthesizes high resolution images by leveraging Poisson blending [22]. In recent years, GAN-based systems have been proposed for synthesis realism in geometry domain [41], [42], [43], [44], e.g., [5] presents a spatial transformer GAN (ST-GAN) by inserting STNs into the generator, Azadi et al. [7] describe a Compositional GAN that introduces a self-consistent composition-decomposition network, Yao et al. [45] study GAN-based 3D manipulation, etc.

Our HIC-GAN incorporates image synthesis in geometry and appearance domains into an end-to-end trainable network and achieves synthesis realism in both domains simultaneously. It requires no supervision and is capable of composing images with multiple foreground objects with or without occlusion, more detail to be described in the ensuing Section on Proposed Method.

III. PROPOSED METHOD

The proposed HIC-GAN consists of a geometry module as shown in Fig. 2 and an appearance module as shown in Fig. 3 that are inter-connected and end-to-end trainable.

A. Geometry Module

The geometry module as shown in Fig. 2 aims to compose the foregrounds and background in geometry domain with realistic spatial layout and occlusion relationship. The geometry module contains two branches to achieve the spatial alignment of multiple objects and deal with the occlusion relationship, respectively.

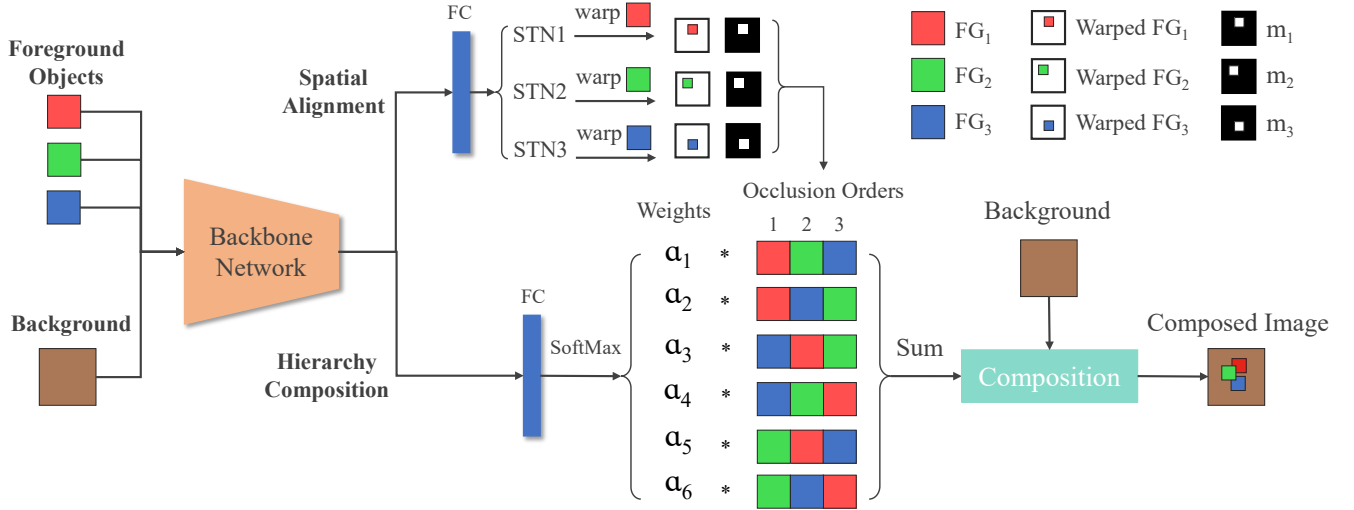


Fig. 2. The framework of geometry module which consists of a spatial alignment branch and a hierarchy composition branch. In the spatial alignment branch, three separated spatial transform networks (STN1, STN2, STN3) are employed to achieve spatial alignment between multiple foreground objects (FG_1, FG_2, FG_3). The hierarchy composition branch aims to explicitly identify the occlusion relationship between foreground objects. Specially, there are six types of possible occlusion relationships between three foreground objects. Thus six weight parameters ($\alpha_1, \dots, \alpha_6$) are predicted to indicate the probability of each occlusion relationship. The numbers 1,2,3 in occlusion orders denote the occlusion priority from high to low. The summation of all possible occlusion results will compose with the background to form the composed image.

At first, the foreground objects and background image are concatenated to act as the input of backbone network (DenseNet121 [46] in our work). In the spatial alignment branch, the feature extracted by the backbone network is further fed into three spatial transform networks [47] (STN1, STN2, STN3) to predict transformation parameters to warp foreground objects, thus achieving the spatial alignment of multiple foreground objects. The transformation types can be affine, homography, or thin plate spline [48] (We use thin plate spline for scene text synthesis task and homography for portrait editing and indoor rendering tasks).

Besides the spatial layout of foreground objects, the occlusion relationship between foreground objects also significantly affect the visual realism. We thus introduce hierarchy composition branch to explicitly identify the occlusion relationship between foreground objects to be introduced as below.

Hierarchy Composition Mechanism: As shown in Fig. 2, for three foreground objects, there are six types of possible occlusion relationship. Thus six weights ($\alpha_1, \dots, \alpha_6$) are predicted to indicate the occlusion relationship between foreground objects. Each type of occlusion relationship results in a composition result, and the weighted summation of six types of composition results forms the finally composed image. To derive the formula of finally composed image, we denote three warped foreground objects as FG_1, FG_2, FG_3 , three binary masks of foreground objects as m_1, m_2, m_3 , and use ‘>’ to denote their occlusion relationship (namely $FG_i > FG_j$ means FG_i occludes FG_j). Considering an occlusion scenario $FG_1 > FG_2 > FG_3$, the corresponding occlusion result O_1 can be derived by:

$$O_1 = FG_1 * m_1 + FG_2 * (m_2 - m_2 \cap m_1) + FG_3 * (m_3 - (m_3 \cap m_1) \cup (m_3 \cap m_2)) \quad (1)$$

The weighted summation of all possible occlusion results will

compose with the background to form the composed image C as below:

$$C = \sum_{i=1}^6 (O_i * \alpha_i) + BG * (1 - m_1 \cup m_2 \cup m_3) \quad (2)$$

To extend the hierarchy composition mechanism to M foreground objects, we denote the foreground objects as FG_1, \dots, FG_M , the corresponding foreground mask as m_1, \dots, m_M . With M foreground objects, there are $A_M^M = M * (M-1) * \dots * 2 * 1$ possible occlusion scenarios, thus A_M^M weight parameters are predicted as denoted by $\alpha_1, \dots, \alpha_{A_M^M}$. Taking one scenario $FG_1 > FG_2 > \dots > FG_{M-1} > FG_M$ with a weight of α_1 as an example, the occlusion result in this scenario can be derived by:

$$O_1 = FG_1 * m_1 + FG_2 * (m_2 - m_2 \cap m_1) + \dots + FG_M * (m_M - (m_M \cap m_1) \cup (m_M \cap m_2) \dots \cup (m_M \cap m_{M-1})) \quad (3)$$

The weighted summation of all possible image compositions $C_{FG_{n_1} > FG_{n_2} \dots FG_{n_M}} (n_1 \neq n_2 \dots \neq n_M)$ forms the ‘Composed Image’ C as follows:

$$C = \sum_{i=1}^{A_M^M} (O_i * \alpha_i) + BG * (1 - m_1 \cup m_2 \cup \dots \cup m_M) \quad (4)$$

The learning of weight parameters is driven by D_2 in the appearance module (to be introduced in the ensuing section) as shown Fig. 3. Note the training references of the geometry module are not real images which are realistic in both geometry and appearance. As the geometry module seeks synthesis realism in geometry domain, the appearance realism in natural images becomes certain noises which could mislead the geometry learning in adversarial training. For the geometry

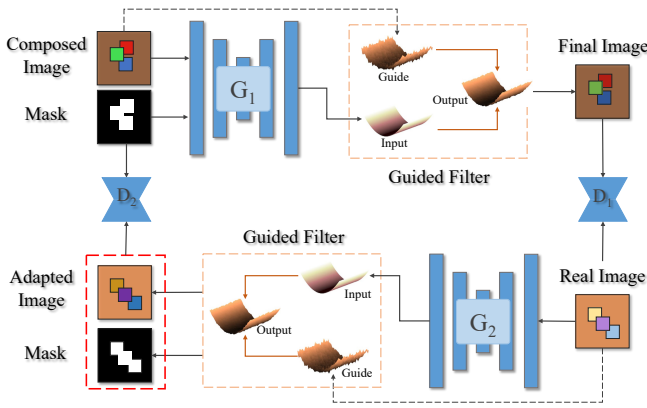


Fig. 3. The structure of appearance module: D_1 , D_2 , G_1 , G_2 denote two discriminators and two generators. The components in the dotted orange-color boxes denote guided filters. G_1 maps from Composed Image to Final Image and G_2 maps from Real Image to Adapted Image. The input of D_1 is the concatenation of the Composed Image and the corresponding Mask. The images in the dotted red-color boxes denote the training reference for the geometry module.

module, the ideal training reference should be realistic in geometry domain while fake in appearance domain as shown in the ‘Adapted WM’ in Fig. 4. We derive such references by using the output of the appearance module as denoted by red box in Fig. 3 which will be described in the ensuing subsection.

B. Appearance Module

The appearance module employs a cycle structure to translate the foreground objects to be harmonious with the background image as shown in Fig. 3. It employs two generators G_1 and G_2 for image-to-image translation in reverse directions. G_1 tries to translate the Composed Image to Final Image, while G_2 tries to generate Adapted Image and the corresponding mask from Real Image. Two discriminators D_1 and D_2 are adopted to distinguish the generated images and corresponding training references in the reverse mappings.

Specifically, D_1 strives to distinguish Final Image and Real Image which guides G_1 to learn the realistic translation of appearance. At the other end, D_2 learns to distinguish the Composed Image and Adapted Image, aiming to generate Adapted Image that is realistic in geometry domain but have similar appearance to the Composed Image as shown in Fig. 4. As mentioned in the previous subsection, HIC-GAN uses the Adapted Image generated by G_2 as the reference to train the geometry module so that it can focus on synthesizing more realistic image geometry (as the interfering appearance differences have been suppressed between Adapted Image and Composed Image).

Guided Filter: As appearance transfer in most image-to-image-translation GANs tends to sacrifice image details, we introduce guided filters [25], [49] into the appearance module for detail preservation as shown in Fig. 3. Guided Filter computes the filtering output by using a guidance image that can be the input image itself or another different image. It can thus be formulated as a joint up-sampling problem that

up-samples the filtering image under the guidance of another image.

For clarity, we denote the Composed Image and the corresponding Mask in Fig. 3 as y and y_m , the Final Image as y_{ad} , the Real Image as z , the Adapted Image and the corresponding Mask as z_{ad} and z_m . For the mapping from y, y_m to y_{ad} , the Composed Image y (image details unchanged) acts as the guide to provide edge and texture details, and the output of G_1 (image details lost) as denoted by $G_1(y)$ acts as the input that provides translated appearance information (contrast, illumination and so on). The Final Image y_{ad} with preserved details can be derived by minimizing the reconstruction error between $G_1(y)$ and y_{ad} , subjects to a linear model as follows:

$$y_{ad}^i = a_k G_1(y)^i + b_k, \forall i \in \omega_k \quad (5)$$

where i denotes the index of a pixel and k denotes the index of a local square window ω_k with a radius r . Coefficients a_k and b_k can be estimated by minimizing the difference between y_{ad} and y which can be derived by minimizing the following cost function within ω_k :

$$E(a_k, b_k) = \sum_{i \in \omega_k} ((a_k G_1(y)^i + b_k - y^i)^2 + \varepsilon a_k^2) \quad (6)$$

where ε is a regularization parameter that prevents a_k from being too large. It can be solved via linear regression:

$$a_k = \frac{\frac{1}{|\omega|} \sum_{i \in \omega_k} G_1(y)^i y^i - \mu_k \bar{y}_k}{\sigma_k^2 + \varepsilon}, \quad b_k = \bar{y}_k - a_k \mu_k \quad (7)$$

where μ_k and σ_k^2 are the mean and variance of y within ω_k , $|\omega|$ is the number of pixels in ω_k , and $\bar{y}_k = \frac{1}{|\omega|} \sum_{i \in \omega_k} y_i$ is the mean of y within ω_k .

By computing (a_k, b_k) for every pixel, the filter output can be derived by averaging all possible values of y_{ad}^i :

$$y_{ad}^i = \frac{1}{|\omega|} \sum_{k: i \in \omega_k} (a_k G_1(y)^i + b_k) = \bar{a}_i y_i + \bar{b}_i \quad (8)$$

where $\bar{a}_i = \frac{1}{|\omega|} \sum_{k: i \in \omega_k} a_k$ and $\bar{b}_i = \frac{1}{|\omega|} \sum_{k: i \in \omega_k} b_k$. The guide filters are embedded into the cycle network structure to implement an end-to-end trainable system.



Fig. 4. ‘Adapted WM’ and ‘Adapted W/o M’ denote ‘Adapted Image’ (in Fig. 3) from ‘Real Images’ with and without using attention masks. Adapted images are better training reference for the geometry module compared with ‘Real Images’, because the discrepancy in appearance domain between the ‘Composed Images’ and adapted images are suppressed, thus driving the adversarial learning to focus on geometric learning.

Attention Mask: The image translation in G_1 , and G_2 is conducted on full image which also translates undesired regions beyond the foreground region. Specifically, G_2 cannot generate Adapted Image z_{ad} precisely from Real Image z as it needs to identify the foreground region in Real Image at first. To constrain the appearance transfer within the foreground region, we introduce binary attention masks as denoted by y_m (for Composed Image) and z_m (for Adapted Image) which are concatenated with the Composed Image and Adapted Image as the input of G_1 and D_2 in training. With the attention mask, G_1 is able to adapt the foreground region of the composed image accurately and compress undesired translation of other regions. In addition, the attention mask is also applied to adjust the weight of the cycle-consistency loss of different regions to be introduced in the ensuing section.

Note G_2 generates z_{ad} and z_m under certain supervision. Specifically, y_m is a mask (ground truth) of Composed Image y as produced by the geometry module, where y and y_m are translated by G_1 to obtain the Final Image y_{ad} . With the cycle-consistency loss, y_{ad} is further fed into G_2 to recover y and y_m . As the ground truth of y_m and y is available from the geometry module, the generation of attention mask in G_2 is actually supervised to some sense. As Fig. 4 shows, with the attention mask mechanism, G_2 tends to translate the foreground region of Real Image accurately, thus providing better training reference for the geometry module. On the other hand, the Composed Image with better geometric realism will enable the appearance module to concentrate on the adaptation in appearance domain. The two modules thus collaborate and drive each other for the optimal synthesis.

C. Adversarial Training

The geometry module and appearance module are actually two inter-connected GANs that collaborate with each other during training. Thus HIC-GAN employs two adversarial objectives to achieve realism in both geometry and appearance domains. For clarity, we denote the input of the geometry module, the ‘Composed Image’ and the ‘Real Image’ as x , y and z , and the corresponding image domains by X , Y and Z , respectively.

In geometry module, the network performs as a specific generator C which generates images by composing foreground objects and background image. We adopt the Wasserstein GAN [2] objective to train the network with an iterative updating strategy [5] of transformation parameters. Thus the loss functions of S and D_2 are formulated by:

$$\begin{aligned} \mathcal{L}_{D_2} &= E_{x \sim X}[D_2(S(x))] - E_{z_{ad} \sim Z_{ad}}[D_2(z_{ad}, z_m)] \\ \mathcal{L}_S &= -E_{x \sim X}[D_2(S(x))] \end{aligned} \quad (9)$$

where z_{ad} and z_m denote the ‘Adapted Image’ and the corresponding ‘Mask’.

The appearance module adopts a cycle structure that involves two mappings in the reverse directions. The learning objective consists of an adversarial loss for cross-domain mapping and a cycle consistency loss that prevents mode

TABLE I
EVALUATION OF PORTRAIT EDITING: THE AMT SCORE NUMBERS DENOTE THE PERCENTAGE OF IMAGES THAT ARE CLASSIFIED AS REAL BY TURKERS. MS DENOTES MANIPULATION SCORE [50].

Methods	AMT Score \uparrow	MS \downarrow	FID \downarrow
UNIT [51]	4%	0.85	120.6
CycleGAN [3]	7%	0.71	79.5
ST-GAN [5]	12%	0.85	40.5
ST-GAN + CycleGAN	29%	0.73	37.4
SF-GAN [6]	35%	0.68	32.7
HIC-GAN	38%	0.64	29.1

collapse. For the adversarial loss, the loss function of D_1 and G_1 can be formulated by:

$$\begin{aligned} \mathcal{L}_{D_1} &= E_{y \sim Y}[D_1(G_1(y, y_m))] - E_{z \sim Z}[D_1(z)] \\ \mathcal{L}_{G_1} &= -E_{y \sim Y}[D_1(G_1(y, y_m))] \end{aligned} \quad (10)$$

where y_m denotes the ‘Mask’ associated with the ‘Composed Image’ y .

To ensure that images can be recovered in the translation cycle and guide the network to focus on foreground objects, an attentional cycle-consistency loss is designed:

$$\begin{aligned} \mathcal{L}_{G_{1cyc}} &= E_{y \sim Y}[\|(G_2(G_1(y, y_m)) - (y, y_m)) * y_m\|] * \alpha \\ &+ E_{y \sim Y}[\|(G_2(G_1(y, y_m)) - (y, y_m)) * (1 - y_m)\|] \end{aligned} \quad (11)$$

where α denotes the weights of the foreground region.

While updating the appearance module, all weights of the geometry module are frozen. For the mapping from Composed Image to Final Image, \mathcal{L}_{D_1} and $\mathcal{L}_{G_1} + \lambda \mathcal{L}_{G_{1cyc}}$ are optimized alternately where λ denotes the weight of the cycle-consistency loss. The optimization for the mapping from Real Image to Adapted Image is performed similarly.

IV. EXPERIMENTS

A. Datasets

The proposed HIC-GAN is evaluated over three image synthesis tasks on automated portrait editing, scene text image generation and automated indoor rendering. A number of public datasets are employed in experiments which include:

CelebA [52] is a face image dataset that consists of more than 200k celebrity images with 40 attribute annotations. This dataset is characterized by large quantities, large face pose variations, complicated background clutters, rich annotations, and it is widely used for face attribute prediction.

SUNCG [53] is a Large 3D Model Repository for Indoor Scenes. It is an ongoing effort to establish a richly-annotated large-scale dataset of 3D scenes. The dataset contains over 45K different scenes with manually created realistic rooms and furniture layouts.

ICDAR2013 [54] is used in the Robust Reading Competition in the International Conference on Document Analysis and Recognition (ICDAR) 2013. It contains 848 word images for network training and 1095 for testing.

ICDAR2015 [55] is used in the Robust Reading Competition under ICDAR 2015. It contains incidental scene text

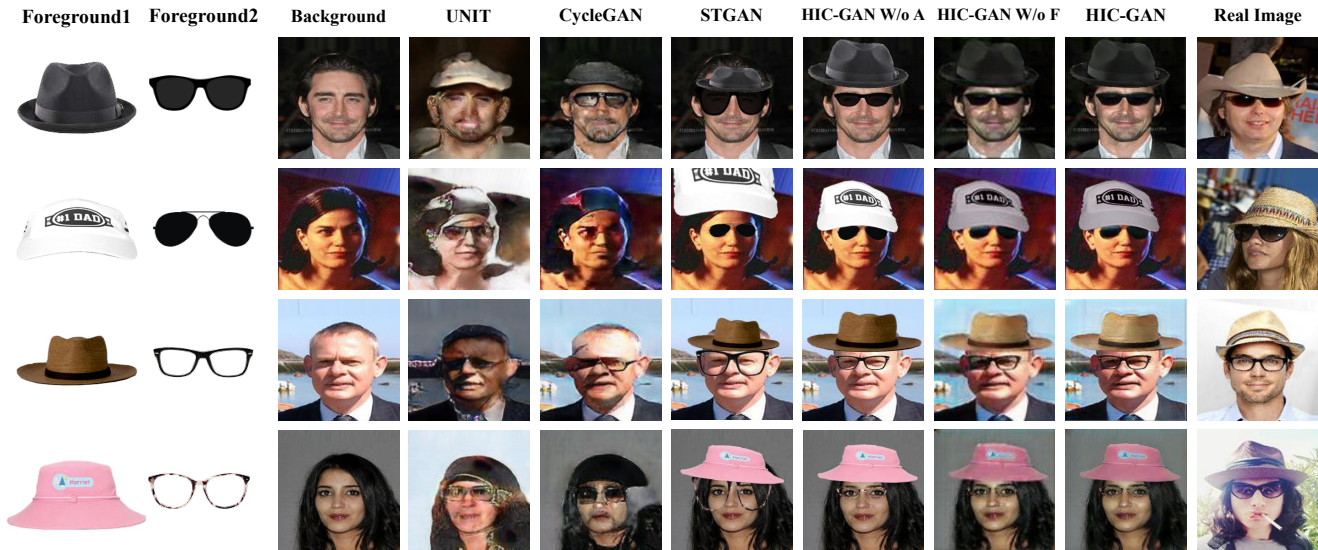


Fig. 5. Comparison of HIC-GAN and its variants with other GANs: HIC-GAN can generate more realistic images with correct occlusions when multiple objects are to be composed. HIC-GAN W/o A denotes the synthesis without appearance module, HIC-GAN W/o F denotes the synthesis without guided filter.

images that are captured without preparation before capturing. 2077 text image patches are cropped from this dataset, where a large amount of cropped scene texts suffer from perspective and curvature distortions.

IIIT5K [56] has 2000 training images and 3000 test images that are cropped from scene texts and born-digital images. Each word in this dataset has a 50-word lexicon and a 1000-word lexicon, where each lexicon consists of a ground-truth word and a set of randomly picked words.

SVT [57] is collected from the Google Street View images that were used for scene text detection research. 647 words images are cropped from 249 street view images and most cropped texts are almost horizontal.

SVTP [58] has 639 word images that are cropped from the SVT images. Most images suffer from perspective distortion which are purposely selected for evaluations.

CUTE [59] has 288 word images. All words are cropped from the CUTE dataset which contains 80 scene text images that are collected for scene text detection research.

B. Implementation

The proposed HIC-GAN is trained on two NVIDIA GTX 1080TI GPUs with 11GB memory. For input image of size 256×256 , it takes 132ms and 96ms per image in training and testing with a batch size of 4. The high efficiency is largely attributed to the introduction of guided filters. Specifically, guided filters can preserve the resolution of the input images effectively and so a generator of small size is sufficient which helps to reduce the network size and time costs greatly.

Homography is adopted as transformation in STN for portrait editing and indoor rendering, and thin plate spline for the scene text synthesis experiment. Although the end-to-end pipeline is not fully convolutional due to the use of STN, the trained model can deal with images of different sizes. As input size of the STN is fixed to 256×256 , the testing image with different sizes will be resized to 256×256 to predict spatial

transformation parameters. The spatial transformation can be applied on the image of original size instead of the resized image, so we can obtain composed image of the original size. As the appearance module is fully convolutional, the end-to-end model can deal with image of arbitrary sizes.

As the original CycleGAN [3] and UNIT [51] were not designed for image composition, we apply them to achieve image-to-image translation from the background images to the training reference. The original ST-GAN [5] and SF-GAN [6] can compose with a single object only and we extend it for multiple objects by composing each object iteratively. There are two foreground objects for the portrait editing experiment, two foreground objects for scene text synthesis experiment and three foreground objects for indoor rendering experiment.

C. Portrait Editing

Experimental Setting: We test portrait editing on CelebA [52] and follow the provided training/test split in experiments. With the attribute annotations, we extract 3000 faces without hat and glasses as the background images and 3000 faces with hat and glasses as training references. For foreground objects, we use 20 cropped hats and 20 cropped glasses to compose with randomly selected background images. The hat and glasses are not paired with the faces, and the composed images are not paired with training reference either.

Results Analysis: We compare HIC-GAN with state-of-the-art GANs including SF-GAN[6], UNIT[51], CycleGAN[3], ST-GAN[5] and the combination of CycleGAN and ST-GAN on portrait editing task as shown in Table I. The combination of CycleGAN and ST-GAN aims to take care of both appearance and geometry in synthesis, where images are firstly composed by ST-GAN and then translated by CycleGAN. The comparison were performed by using FID [60], Manipulation score [50] and Amazon Mechanical Turk (AMT) where 20 users are recruited to tell whether the synthesized images (100 images

TABLE II

EVALUATION OF SYNTHESIZED IMAGES ON SCENE TEXT RECOGNITION: THE EXPERIMENTS ARE CONDUCTED OVER SIX DATASETS INCLUDING ICDAR2013, ICDAR2015, IIIT5K, SVT, SVTP AND CUTE AS LISTED IN THE FIRST ROW, WHERE 1 MILLION TEXT IMAGES SYNTHESIZED BY EACH METHOD ARE USED IN NETWORK TRAINING.

Methods	ICDAR2013	ICDAR2015	IIIT5K	SVT	SVTP	CUTE	Average
Jaderberg et al.[15]	70.1	55.4	79.8	78.4	65.1	56.3	67.5
Gupta et al. [14]	80.9	51.8	79.0	68.0	53.4	47.6	63.5
Zhan et al.[16]	81.4	54.7	80.2	77.7	65.0	56.7	69.3
ST-GAN [5]	64.7	34.1	48.9	49.5	34.7	32.1	44.0
CycleGAN+ST-GAN	66.6	41.6	54.5	56.5	42.3	32.1	48.9
SF-GAN[6]	81.2	55.5	81.3	79.2	64.9	57.3	69.9
HIC-GAN	83.9	57.8	82.3	81.2	66.8	59.1	71.85

TABLE III

EVALUATION OF SCENE TEXT IMAGE SYNTHESIS: THE AMT SCORE NUMBERS DENOTE THE PERCENTAGE OF IMAGES THAT ARE CLASSIFIED AS REAL BY TURKERS. MS DENOTES MANIPULATION SCORE [50].

Methods	AMT Score \uparrow	MS \downarrow	FID \downarrow
UNIT [51]	2%	0.79	76.1
CycleGAN [3]	3%	0.73	51.2
ST-GAN [5]	10%	0.83	27.4
ST-GAN + CycleGAN	27%	0.74	25.2
SF-GAN [6]	37%	0.66	21.9
HIC-GAN	39%	0.62	18.4

synthesized by each method) are real or not (The same AMT setting for Table III and IV). As Table I shows, HIC-GAN outperforms all compared GANs in AMT score, manipulation score and FID consistently.

Fig. 5 compares the portrait editing of different methods qualitatively. As shown in Fig. 5, the HIC-GAN synthesized images are much more realistic than those synthesized by other methods. Specifically, HIC-GAN correctly learns the occlusion relationship between the hat and glasses. CycleGAN [3] and UNIT [51] can achieve certain realism in appearance domain, but the synthesized images are blurry and present low image quality. ST-GAN [5] can preserve the image quality and perform geometric transformation, but the learned geometric transformation is not accurate in term of object size and embedding locations. In addition, it cannot handle synthesis realism in appearance domain.

D. Scene Text Synthesis

Experimental Setting: For scene text image synthesis, HIC-GAN requires a set of background images and foreground texts and also requires real scene text images as ground truth. We collect the scene text images by cropping from the training images of ICDAR2013 [54], ICDAR2015 [55], SVT [57] and CUTE [59]. For the background images, we collect them by performing image inpainting to the cropped image to erase the scene texts as illustrated in ‘BG’ in Fig. 6. The foreground text is randomly selected from the 90k-lexicon [15].

Besides AMT, manipulation score and FID, we use accuracy of scene text recognition models (trained using synthesized images) to evaluate image synthesis methods. Specifically, we

synthesize 1 million images by HIC-GAN and several state-of-the-art synthesis methods (Jaderberg et al. [15], Gupta et al. [14], Zhan et al. [16]) as well as several GANs (SF-GAN [6], ST-GAN and the combination of ST-GAN and CycleGAN [3]). MORAN [61] is used as text recognition model which is trained by using the images synthesized with the compared methods. The trained models are tested over six datasets ICDAR2013 [54], ICDAR2015 [55], IIIT5K [56], SVT [57], SVTP [58] and CUTE [59] as described in **Datasets**. Word level accuracy is used to evaluate the quality of the training images as synthesized by different methods.



Fig. 6. Illustration of scene text image synthesis by different GANs: ‘BG’ in Row 1 denotes the background images. Rows 2-4 show the images that are synthesized by UNIT, CycleGAN and ST-GAN, respectively. Row 5 shows the images synthesized by HIC-GAN with 2 foreground text instances.

Results Analysis: Table II shows scene text recognition accuracy by different synthesis methods. As Table II shows, HIC-GAN achieves the highest recognition accuracy for the six evaluated datasets. In addition, it achieves an up to 2% improvement over SF-GAN [6] across the six datasets, demonstrating the superior usefulness of its synthesized images in training scene text recognition models. Besides, Table III compares the AMT scores, manipulation scores and FID of different methods and HIC-GAN outperforms other methods consistently. The better performance is largely attributed to the attention masks which helps achieve better synthesis geometry by providing better training references (i.e. ‘Adapted Image’ in Fig. 3). Additionally, the attention masks as the input of the discriminator also provide additional geometry information to

TABLE IV

EVALUATION OF INDOOR RENDERING: THE AMT SCORE NUMBERS DENOTE THE PERCENTAGE OF IMAGES THAT ARE CLASSIFIED AS REAL BY TURKERS. MS DENOTES MANIPULATION SCORE [50].

Methods	AMT Score \uparrow	MS \downarrow	FID \downarrow
UNIT [51]	1%	0.80	61.5
CycleGAN [3]	4%	0.71	48.6
ST-GAN [5]	8%	0.80	25.7
ST-GAN + CycleGAN	24%	0.73	23.8
SF-GAN [6]	38%	0.65	21.2
HIC-GAN	41%	0.63	17.6

the training of the geometry module. Note scene text images with multiple text instances cannot be synthesized by applying existing GANs multiple times. The reason is the lack of coordination among multiple executions, where each execution seeks the best embedding region for the current text instance without considering other executions.

Fig. 6 shows the scene text images synthesized by different methods. For UNIT [51] and CycleGAN [3], we directly apply them to perform image-to-image translation from background images to real images. As Fig. 6 shows, UNIT tends to generate images with messy strokes. CycleGAN can generate strokes with real appearance but the generated strokes have no semantic meaning. Besides, both methods do not generate any annotation information. ST-GAN [5] learns poor geometry transformations, largely because it uses real images as references where the appearance realism in real images misleads the network training. HIC-GAN can synthesize scene text images with two text instances as shown in Fig. 6. It correctly aligns the spatial layout of different text instances, where different spatial transformations are learned and applied according to the local geometry. At the same time, the appearance of the embedded text instances is adapted to be harmonious with the contextual backgrounds.

E. Indoor Rendering

Experimental Setting: The indoor rendering aims to compose furniture in indoor scenes. The dataset for indoor rendering is created from SUNG dataset [53] that contains 41,499 scene models and 568,749 camera viewpoints from [62] and [63]. To achieve multiple objects composition in indoor rendering, we select bed, sofa and shelf as foreground objects and images with bed, sofa and shelf as the training references. The rendering pipeline for indoor data is consistent with the framework described in ST-GAN [5].

Results Analysis: We evaluate HIC-GAN and compare it with SF-GAN [6], ST-GAN [5], CycleGAN [3] and the combination of ST-GAN and CycleGAN in AMT user study, Manipulation scores and FID. Table IV shows experimental results. It can be observed that HIC-GAN outperforms all compared methods clearly and consistently. Note we apply random brightness change to the foreground objects which disturbs the ST-GAN training by the discrepancy in the appearance and leads to lower AMT scores than those reported in [5]. HIC-GAN outperforms SF-GAN by 4%, largely due to the attention

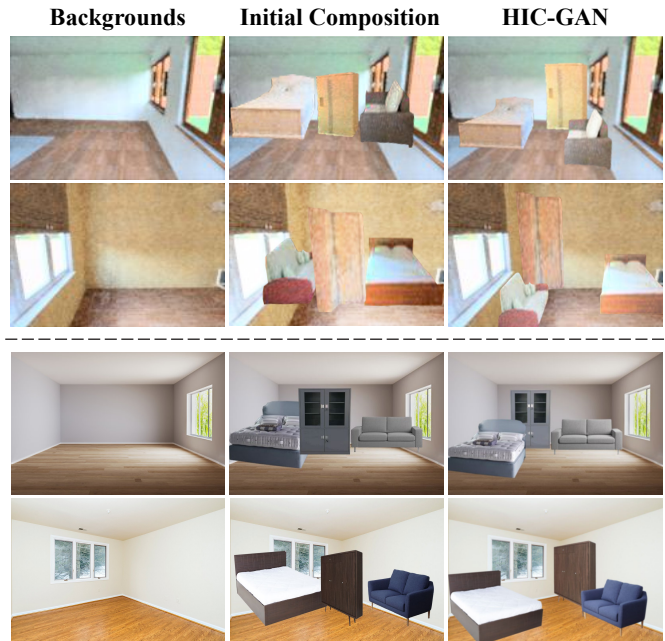


Fig. 7. The first and last two rows shows the indoor rendering on the testing set and the real scene set, respectively. ‘Initial’ denotes initially composed images without any alignment.

mask that generate more realistic Adapted Image and Mask (in Fig. 3) which as training reference further helps the geometry module learn more realistic geometry than SF-GAN.

The first two rows of Fig. 7 show the indoor rendering on the testing set that is created from SUNCG dataset. As the foreground objects are not paired with the background, the initially composed images ‘Initial Composition’ tend to be fake in both geometry and appearance with unrealistic occlusions. HIC-GAN learns the geometry of background to align the foreground objects realistically and adapts their appearance with overall harmonization. It also learns the correct occlusions among foreground objects, generating much more realistic images than the initially composed images. We also evaluate HIC-GAN on the real scene images as shown in the last two rows of Fig. 7 which are collected from the Internet by cropping the foreground objects and selecting the background images manually. As shown in Fig. 7, HIC-GAN embeds foreground objects with realistic geometry and occlusion and adapts their appearance to be harmonious with the background images.

F. Ablation Study

We conduct ablation study on the portrait editing task with four HIC-GAN variants as shown in Table V, where each cell has two percentages telling which of the paired images synthesized by Methods A or B are more realistic (100 pairs of images are presented to 20 users for judgment). HIC-GAN (W/o A) denote HIC-GAN without the proposed appearance module. It has much lower AMT scores than the standard HIC-GAN, demonstrating the importance of appearance realism in image composition. Nevertheless, it outperforms ST-GAN with AMT score 60% versus 40%, largely due to the use of

TABLE V

ABLATION STUDY OVER THE PORTRAIT EDITING TASKS (IN AMT): EACH CELL CONTAINS TWO PERCENTAGES THAT TELL WHICH OF PAIRED IMAGES SYNTHESIZED BY METHODS A AND B (IN THE FORMAT OF ‘METHOD A’ - ‘METHOD B’) ARE DEEMED AS MORE REALISTIC BY USERS. HIC-GAN (W/O A), HIC-GAN (W/O H), HIC-GAN (W/O M), HIC-GAN (W/O F) DENOTE HIC-GAN WITHOUT APPEARANCE MODULE, HIERARCHY COMPOSITION MECHANISM, ATTENTION MASK AND GUIDED FILTER, RESPECTIVELY.

Method A \ Method B	Baseline	UNIT	CycleGAN	ST-GAN	CycleGAN+ST-GAN	SF-GAN	Real
HIC-GAN (W/o A)	83%-17%	53%-47%	46%-54%	60%-40%	38%-62%	28%-72%	19%-81%
HIC-GAN (W/o H)	96%-4%	81%-19%	66%-34%	77%-23%	60%-40%	52%-48%	31%-69%
HIC-GAN (W/o M)	95%-5%	87%-13%	72%-28%	82%-18%	62%-38%	55%-44%	36%-64%
HIC-GAN (W/o F)	100%-0%	90%-10%	76%-24%	88%-12%	68%-32%	59%-41%	41%-59%
HIC-GAN	100%-0%	92%-8%	79%-21%	89%-11%	73%-27%	61%-39%	42%-58%

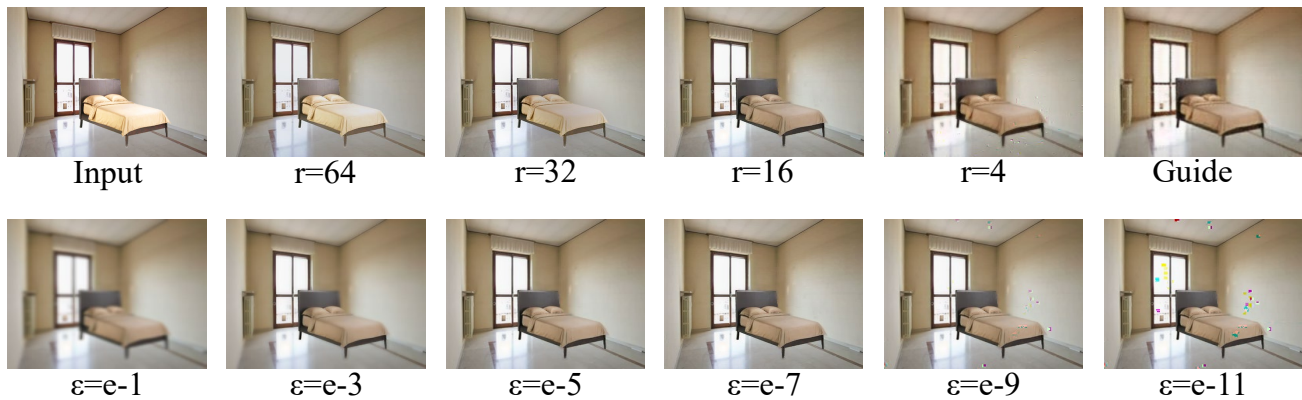


Fig. 8. The effect of radius r and regularization ϵ in guided filter: ‘Input’ and ‘Guide’ denote the input image and guide image. Row 1 shows the synthesis with different r (ϵ fixed at $e-7$), and Row 2 shows the synthesis with different ϵ (r fixed at 16).

‘Adapted Image’ which improve synthesis realism in geometry domain. HIC-GAN (W/o M) denotes HIC-GAN without using attention masks. Its AMT scores are clearly lower than the standard HIC-GAN because attention masks help generate better appearance adaptation. HIC-GAN (W/o H) denotes HIC-GAN without the hierarchy composition mechanism. As shown in Table V, (W/o H) has lower AMT scores than Standard HIC-GAN, demonstrating that correct occlusion relationship between foreground objects affects the synthesis realism greatly. HIC-GAN (W/o F) denotes HIC-GAN without using the guided filter. The corresponding AMT scores are slightly lower than that of standard HIC-GAN as guided filters mainly help to preserve image resolution and details but don’t contribute much to the synthesis realism.

In the indoor rendering experiment, we further explore the role of radius r and regularization ϵ as described in Section III-B **Guided Filter**, where r controls the bandwidth of the guided filter and ϵ controls the degree of edge preservation. To simply the scenario, the experiment is conducted with a single foreground object. As Fig. 8 shows, the filter output with a large r tends to be similar to the ‘Input’ with high resolution, but its appearance does not change much and tends to be unrealistic. When r becomes smaller, the filter output is translated towards the ‘Guide’ in appearance. At the other end, the resolution of the filter output decreases when r becomes smaller. For the regularization ϵ , the filter output tends to be blurry and loses details when ϵ is large. With the decrease of

ϵ , the filter output preserves more details but certain noises are introduced. Certain trade-off needs to be taken for r and ϵ depending on specific requirements. In our implemented system, we set r and ϵ at 16 and $e-7$ empirically.

V. CONCLUSIONS

This paper presents HIC-GAN, an end-to-end trainable network that composes images with multiple foreground objects. HIC-GAN consists of a geometry module and an appearance module that collaborate to achieve synthesis realism in geometry and appearance domains simultaneously. A novel hierarchy composition mechanism is designed to handle the occlusion among multiple foreground objects, and an attention mask is exploited to guide the appearance adaptation and provide better training reference for the geometry module. Extensive experiments on portrait editing, scene text synthesis and indoor rendering show that the proposed HIC-GAN can compose both high-fidelity images and useful images for deep model training. The proposed HIC-GAN mainly works with 2-dimensional (2D) images which is constrained by very limited views of the foreground objects. We will explore image synthesis in 3-dimensional (3D) space for better synthesis flexibility and synthesis realism in our future work.

VI. ACKNOWLEDGEMENT

This work is funded by the Ministry of Education (MOE), Singapore, under the project ‘‘A semi-supervised learning

approach for accurate and robust detection of texts in scenes” (RG128/17 (S)).

REFERENCES

- [1] I. J. Goodfellow, J. Pouget-Abadie, M. Mirza, B. Xu, D. Warde-Farley, S. Ozair, A. Courville, and Y. Bengio, “Generative adversarial networks,” in *NIPS*, 2014, pp. 2672–2680.
- [2] M. Arjovsky, S. Chintala, and L. Bottou, “Wasserstein generative adversarial networks,” in *International Conference on Machine Learning*, 2017, pp. 214–223.
- [3] J.-Y. Zhu, T. Park, P. Isola, and A. A. Efros, “Unpaired image-to-image translation using cycle-consistent adversarial networks,” in *Proceedings of the IEEE international conference on computer vision*, 2017, pp. 2223–2232.
- [4] P. Isola, J.-Y. Zhu, T. Zhou, and A. A. Efros, “Image-to-image translation with conditional adversarial networks,” in *Proceedings of the IEEE conference on computer vision and pattern recognition*, 2017, pp. 1125–1134.
- [5] C.-H. Lin, E. Yumer, O. Wang, E. Shechtman, and S. Lucey, “Stgan: Spatial transformer generative adversarial networks for image compositing,” in *Proceedings of the IEEE Conference on Computer Vision and Pattern Recognition*, 2018, pp. 9455–9464.
- [6] F. Zhan, H. Zhu, and S. Lu, “Spatial fusion gan for image synthesis,” in *Proceedings of the IEEE conference on computer vision and pattern recognition*, 2019, pp. 3653–3662.
- [7] S. Azadi, D. Pathak, S. Ebrahimi, and T. Darrell, “Compositional gan: Learning image-conditional binary composition,” *arXiv preprint arXiv:1807.07560*, 2018.
- [8] Y. Movshovitz-Attias, T. Kanade, and Y. Sheikh, “How useful is photo-realistic rendering for visual learning?” in *European Conference on Computer Vision*. Springer, 2016, pp. 202–217.
- [9] D. Park and D. Ramanan, “Articulated pose estimation with tiny synthetic videos,” in *Proceedings of the IEEE Conference on Computer Vision and Pattern Recognition Workshops*, 2015, pp. 58–66.
- [10] H. Su, C. R. Qi, Y. Li, and L. J. Guibas, “Render for cnn: Viewpoint estimation in images using cnns trained with rendered 3d model views,” in *Proceedings of the IEEE International Conference on Computer Vision*, 2015, pp. 2686–2694.
- [11] A. Gaidon, Q. Wang, Y. Cabon, and E. Vig, “Virtual worlds as proxy for multi-object tracking analysis,” in *Proceedings of the IEEE conference on computer vision and pattern recognition*, 2016, pp. 4340–4349.
- [12] S. R. Richter, V. Vineet, S. Roth, and V. Koltun, “Playing for data: Ground truth from computer games,” in *European conference on computer vision*. Springer, 2016, pp. 102–118.
- [13] J.-Y. Zhu, P. Krahenbuhl, E. Shechtman, and A. A. Efros, “Learning a discriminative model for the perception of realism in composite images,” in *Proceedings of the IEEE International Conference on Computer Vision*, 2015, pp. 3943–3951.
- [14] A. Gupta, A. Vedaldi, and A. Zisserman, “Synthetic data for text localisation in natural images,” in *Proceedings of the IEEE conference on computer vision and pattern recognition*, 2016, pp. 2315–2324.
- [15] M. Jaderberg, K. Simonyan, A. Vedaldi, and A. Zisserman, “Synthetic data and artificial neural networks for natural scene text recognition,” in *Neural Information Processing Systems*, 2014.
- [16] F. Zhan, S. Lu, and C. Xue, “Verisimilar image synthesis for accurate detection and recognition of texts in scenes,” in *Proceedings of the European Conference on Computer Vision (ECCV)*, 2018, pp. 249–266.
- [17] F. Zhan and S. Lu, “Esir: End-to-end scene text recognition via iterative image rectification,” in *Proceedings of the IEEE Conference on Computer Vision and Pattern Recognition*, 2019, pp. 2059–2068.
- [18] F. Zhan, C. Xue, and S. Lu, “Ga-dan: Geometry-aware domain adaptation network for scene text detection and recognition,” in *Proceedings of the IEEE International Conference on Computer Vision*, 2019, pp. 9105–9115.
- [19] F. Zhan, H. Zhu, and S. Lu, “Scene text synthesis for efficient and effective deep network training,” *arXiv preprint arXiv:1901.09193*, 2019.
- [20] D. Dwibedi, I. Misra, and M. Hebert, “Cut, paste and learn: Surprisingly easy synthesis for instance detection,” in *Proceedings of the IEEE International Conference on Computer Vision*, 2017, pp. 1301–1310.
- [21] M. Uyttendaele, A. Eden, and R. Skeliski, “Eliminating ghosting and exposure artifacts in image mosaics,” in *Proceedings of the 2001 IEEE Computer Society Conference on Computer Vision and Pattern Recognition. CVPR 2001*, vol. 2. IEEE, 2001, pp. II–II.
- [22] P. Pérez, M. Gangnet, and A. Blake, “Poisson image editing,” *TOG*, vol. 22, no. 3, 2003.
- [23] F. Luan, S. Paris, E. Shechtman, and K. Bala, “Deep painterly harmonization,” *arXiv:1804.03189*, 2018.
- [24] Y.-H. Tsai, X. Shen, Z. Lin, K. Sunkavalli, X. Lu, and M.-H. Yang, “Deep image harmonization,” in *Proceedings of the IEEE Conference on Computer Vision and Pattern Recognition*, 2017, pp. 3789–3797.
- [25] K. He, J. Sun, and X. Tang, “Guided image filtering,” *TPAMI*, 2013.
- [26] E. L. Denton, S. Chintala, R. Fergus *et al.*, “Deep generative image models using a laplacian pyramid of adversarial networks,” in *Advances in neural information processing systems*, 2015, pp. 1486–1494.
- [27] D. Lee, S. Liu, J. Gu, M.-Y. Liu, M.-H. Yang, and J. Kautz, “Context-aware synthesis and placement of object instances,” in *Advances in neural information processing systems*, 2018, pp. 10393–10403.
- [28] H. Zhang, T. Xu, H. Li, S. Zhang, X. Wang, X. Huang, and D. N. Metaxas, “Stackgan: Text to photo-realistic image synthesis with stacked generative adversarial networks,” in *Proceedings of the IEEE international conference on computer vision*, 2017, pp. 5907–5915.
- [29] H. Zhang, T. Xu, H. Li, S. Zhang, X. Wang, X. Huang, and D. Metaxas, “Stackgan++: Realistic image synthesis with stacked generative adversarial networks,” *TPAMI*, 2018.
- [30] X. Chen, Y. Duan, R. Houthoofd, J. Schulman, I. Sutskever, and P. Abbeel, “Infogan: Interpretable representation learning by information maximizing generative adversarial nets,” in *Advances in neural information processing systems*, 2016, pp. 2172–2180.
- [31] D. Bau, J.-Y. Zhu, H. Stroblert, B. Zhou, J. B. Tenenbaum, W. T. Freeman, and A. Torralba, “Gan dissection: Visualizing and understanding generative adversarial networks,” in *International Conference on Learning Representations*, 2018.
- [32] T.-C. Wang, M.-Y. Liu, J.-Y. Zhu, A. Tao, J. Kautz, and B. Catanzaro, “High-resolution image synthesis and semantic manipulation with conditional gans,” in *Proceedings of the IEEE conference on computer vision and pattern recognition*, 2018, pp. 8798–8807.
- [33] A. Shrivastava, T. Pfister, O. Tuzel, J. Susskind, W. Wang, and R. Webb, “Learning from simulated and unsupervised images through adversarial training,” in *Proceedings of the IEEE conference on computer vision and pattern recognition*, 2017, pp. 2107–2116.
- [34] J.-Y. Zhu, R. Zhang, D. Pathak, T. Darrell, A. A. Efros, O. Wang, and E. Shechtman, “Toward multimodal image-to-image translation,” in *Advances in neural information processing systems*, 2017, pp. 465–476.
- [35] X. Huang, M.-Y. Liu, S. Belongie, and J. Kautz, “Multimodal unsupervised image-to-image translation,” in *Proceedings of the European Conference on Computer Vision (ECCV)*, 2018, pp. 172–189.
- [36] S. Azadi, M. Fisher, V. G. Kim, Z. Wang, E. Shechtman, and T. Darrell, “Multi-content gan for few-shot font style transfer,” in *Proceedings of the IEEE conference on computer vision and pattern recognition*, 2018, pp. 7564–7573.
- [37] T. Park, M.-Y. Liu, T.-C. Wang, and J.-Y. Zhu, “Semantic image synthesis with spatially-adaptive normalization,” in *Proceedings of the IEEE Conference on Computer Vision and Pattern Recognition*, 2019, pp. 2337–2346.
- [38] M.-Y. Liu, X. Huang, A. Mallya, T. Karras, T. Aila, J. Lehtinen, and J. Kautz, “Few-shot unsupervised image-to-image translation,” *arXiv:1905.01723*, 2019.
- [39] J. Yang, A. Kannan, D. Batra, and D. Parikh, “Lr-gan: Layered recursive generative adversarial networks for image generation,” *arXiv preprint arXiv:1703.01560*, 2017.
- [40] H. Wu, S. Zheng, J. Zhang, and K. Huang, “Gp-gan: Towards realistic high-resolution image blending,” *arXiv:1703.07195*, 2017.
- [41] F. Zhan, S. Lu, C. Zhang, F. Ma, and X. Xie, “Adversarial image composition with auxiliary illumination,” in *Proceedings of the Asian Conference on Computer Vision*, 2020.
- [42] F. Zhan, C. Zhang, Y. Yu, Y. Chang, S. Lu, F. Ma, and X. Xie, “Emlight: Lighting estimation via spherical distribution approximation,” *arXiv preprint arXiv:2012.11116*, 2020.
- [43] F. Zhan, S. Lu, C. Zhang, F. Ma, and X. Xie, “Towards realistic 3d embedding via view alignment,” *arXiv preprint arXiv:2007.07066*, 2020.
- [44] F. Zhan and C. Zhang, “Spatial-aware gan for unsupervised person re-identification,” *Proceedings of the International Conference on Pattern Recognition*, 2020.
- [45] S. Yao, T. M. Hsu, J.-Y. Zhu, J. Wu, A. Torralba, B. Freeman, and J. Tenenbaum, “3d-aware scene manipulation via inverse graphics,” in *Advances in neural information processing systems*, 2018, pp. 1887–1898.
- [46] G. Huang, Z. Liu, L. Van Der Maaten, and K. Q. Weinberger, “Densely connected convolutional networks,” in *Proceedings of the IEEE conference on computer vision and pattern recognition*, 2017, pp. 4700–4708.
- [47] M. Jaderberg, K. Simonyan, A. Zisserman, and koray kavukcuoglu, “Spatial transformer networks,” in *NIPS*, 2015.

- [48] F. L. Bookstein, "Principal warps: Thin-plate splines and the decomposition of deformations," *TPAMI*, vol. 11, no. 6, 1989.
- [49] K. He and J. Sun, "Fast guided filter," *arXiv:1505.00996*, 2015.
- [50] B.-C. Chen and A. Kae, "Toward realistic image compositing with adversarial learning," in *Proceedings of the IEEE Conference on Computer Vision and Pattern Recognition*, 2019, pp. 8415–8424.
- [51] M.-Y. Liu, T. Breuel, and J. Kautz, "Unsupervised image-to-image translation networks," in *Advances in neural information processing systems*, 2017, pp. 700–708.
- [52] Z. Liu, P. Luo, X. Wang, and X. Tang, "Deep learning face attributes in the wild," in *Proceedings of the IEEE international conference on computer vision*, 2015, pp. 3730–3738.
- [53] S. Song, F. Yu, A. Zeng, A. X. Chang, M. Savva, and T. Funkhouser, "Semantic scene completion from a single depth image," in *Proceedings of the IEEE Conference on Computer Vision and Pattern Recognition*, 2017, pp. 1746–1754.
- [54] D. Karatzas, F. Shafait, S. Uchida, M. Iwamura, L. G. i Bigorda, S. R. Mestre, J. Mas, D. F. Mota, J. A. Almazan, and L. P. de las Heras, "Icdar 2013 robust reading competition," in *ICDAR*, 2013, pp. 1484–1493.
- [55] D. Karatzas, L. Gomez-Bigorda, A. Nicolaou, S. Ghosh, A. Bagdanov, M. Iwamura, J. Matas, L. Neumann, V. R. Chandrasekhar, S. Lu, F. Shafait, S. Uchida, and E. Valveny, "Icdar 2015 competition on robust reading," in *ICDAR*, 2015, pp. 1156–1160.
- [56] A. Mishra, K. Alahari, and C. Jawahar, "Scene text recognition using higher order language priors," in *BMVC*, 2012.
- [57] K. Wang, B. Babenko, and S. Belongie, "End-to-end scene text recognition," in *2011 International Conference on Computer Vision*. IEEE, 2011, pp. 1457–1464.
- [58] T. Quy Phan, P. Shivakumara, S. Tian, and C. Lim Tan, "Recognizing text with perspective distortion in natural scenes," in *Proceedings of the IEEE International Conference on Computer Vision*, 2013, pp. 569–576.
- [59] A. Risnumawan, P. Shivakumara, C. S. Chan, and C. L. Tan, "A robust arbitrary text detection system for natural scene images," *Expert Systems with Applications*, vol. 41, no. 18, pp. 8027–8048, 2014.
- [60] M. Heusel, H. Ramsauer, T. Unterthiner, B. Nessler, and S. Hochreiter, "Gans trained by a two time-scale update rule converge to a local nash equilibrium," in *Advances in neural information processing systems*, 2017, pp. 6626–6637.
- [61] C. Luo, L. Jin, and Z. Sun, "Moran: A multi-object rectified attention network for scene text recognition," *Pattern Recognition*, vol. 90, pp. 109–118, 2019.
- [62] Y. Zhang, S. Song, E. Yumer, M. Savva, J.-Y. Lee, H. Jin, and T. Funkhouser, "Physically-based rendering for indoor scene understanding using convolutional neural networks," in *Proceedings of the IEEE Conference on Computer Vision and Pattern Recognition*, 2017, pp. 5287–5295.
- [63] W. Jakob, "Mitsuba renderer," in <http://www.mitsuba-renderer.org/>, 2010.